

Automatic machine-learning potential generation scheme and simulation protocol for the LiGePS-type superionic conductors

Jianxing Huang,[†] Linfeng Zhang,[¶] Han Wang,[§] Jinbao Zhao,^{*,†} Jun Cheng,^{*,†}
and Weinan E^{*,¶}

[†]*College of Chemistry and Chemical Engineering, Xiamen University, Xiamen 361005,
China*

[‡]*State Key Laboratory of Physical Chemistry of Solid Surfaces, Xiamen University,
Xiamen 361005, China*

[¶]*Program in Applied and Computational Mathematics, Princeton University, Princeton,
NJ 08544, USA*

[§]*Laboratory of Computational Physics, Institute of Applied Physics and Computational
Mathematics, Fenghao East Road 2, Beijing 100094, P.R. China*

^{||}*Department of Mathematics, Princeton University, Princeton, NJ 08544, USA*

E-mail: jbzhao@xmu.edu.cn; chengjun@xmu.edu.cn; weinan@math.princeton.edu

Abstract

It has been a challenge to accurately simulate Li-ion diffusion processes in battery materials at room temperature using *ab initio* molecular dynamics (AIMD) due to its high computational cost. This situation has changed drastically in recent years due to the advances in machine learning-based interatomic potentials. Here we implement the Deep Potential Generator scheme to *automatically* generate interatomic potentials

for LiGePS-type solid-state electrolyte materials. This increases our ability to simulate such materials by several orders of magnitude without sacrificing *ab initio* accuracy. Important technical aspects like the statistical error and size effects are carefully investigated. We further establish a reliable protocol for accurate computation of Li-ion diffusion processes at experimental conditions, by investigating important technical aspects like the statistical error and size effects. Such a protocol and the automated workflow allow us to screen materials for their relevant properties with much-improved efficiency. By using the protocol and automated workflow developed here, we obtain the diffusivity data and activation energies of Li-ion diffusion that agree well with the experiment. Our work paves the way for future investigation of Li-ion diffusion mechanisms and optimization of Li-ion conductivity of solid-state electrolyte materials.

All-solid-state Li-ion batteries are amongst the most promising candidates for the next-generation rechargeable batteries.¹⁻⁵ Desired solid-state electrolyte (SSE) materials should have high Li⁺ conductivity and wide electrochemical windows. Several groups of promising candidates, with performance competitive to current commercial liquid electrolytes, e.g., Li₁₀GeP₂S₁₂,⁶ Li₇La₃Zr₂O₂,⁷ Li₇P₃S₁₁,⁸ have been reported.

Improvement of SSE performance lies in the fundamental understanding of diffusion mechanisms. The *ab initio* molecule dynamics (AIMD) calculation⁹ has been utilized to investigate the microscopic details of the diffusion processes.¹⁰⁻¹⁵ Unfortunately, due to its high computational cost, AIMD is typically limited to a system size of hundreds of atoms at the time scale of tens of pico-seconds. This makes it practically impossible to accurately estimate the diffusion coefficient of real materials at room temperature. Therefore one often resorts to the extrapolation strategy: assuming that a single Arrhenius relationship applies to a wide temperature range (this implicitly assumes a temperature-independent diffusion mechanism), one can predict the room-temperature ionic conductivity (-40 °C- 80 °C) by extrapolating from the high-temperature data. For example, a typical dataset for this purpose is ionic conductivity data in the temperature range (600 - 1200K) collected from 100400 ps AIMD simulations^{10,11,15} with 2 × 2 × 1 supercells. However, it has been reported that

this extrapolation strategy based on limited AIMD data may lead to deviation from the experiment by two orders of magnitude at room temperature. This issue, in particular when applied to SSE related calculations, has been comprehensively discussed by He et al.¹⁶

Even more problematically, this Arrhenius extrapolation approach loses predictive power when the Arrhenius relationship breaks down, and this was already discussed in detail over 40 years ago.¹⁷ In particular, as shown in Fig. 1 (a), three different transition behaviors of the ionic conductivity with respect to the inverse of the temperature can give rise to three types of superionic conductors. Fig. 1 (b) depicts the experimental transition behaviors of 3 typical Li-ion ionic conductors. The examples of $\text{Li}_{10.05}\text{Ge}_{1.05}\text{P}_{1.95}\text{S}_{12}$ and $\beta\text{-Li}_3\text{PS}_4$ represent the failures of the extrapolation strategy in Type I and II systems. The assumption behind the extrapolation strategy is only applicable to Type III systems.

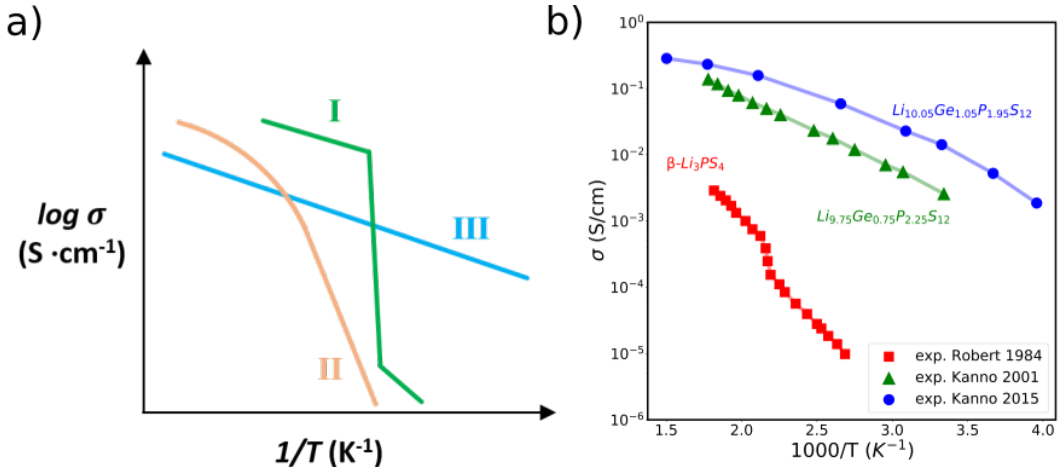


Figure 1: (a) Schematic illustration of the three kinds of the temperature dependence of the conductivity, according to Ref.¹⁷ (b) Temperature dependence of the ionic conductivity of three Li-ion superionic conductors from experiments. Data were taken from the following literature: $\beta\text{-Li}_3\text{PS}_4$,¹⁸ $\text{Li}_{10.05}\text{Ge}_{1.05}\text{P}_{1.95}\text{S}_{12}$ ¹⁹ and $\text{Li}_{9.75}\text{Ge}_{0.75}\text{P}_{2.25}\text{S}_{12}$.²⁰

An obvious solution to the extrapolation problem is to directly simulate the diffusion process at room temperature, which on the other hand requires significantly longer trajectories to ensure convergence of diffusivity data. To accelerate these simulations, there have been ever-increasing efforts to develop empirical potential energy surfaces (PES) or model Hamiltonians involving simple analytical terms, for systems of interest.^{21,22} More recent works have

used machine learning (ML) tools^{5,23–26} to represent the many-body and nonlinear dependence of the PES on atomic positions for materials modeling.^{27–32} In particular, applications to SSE materials, e.g., Li_3PO_4 ,³¹ LiPON,³⁰ and Li_3N ,³² have recently been explored.

Despite these efforts, two major obstacles have remained. First, when the number of chemical species is large, a situation often found for SSE materials, one needs a representation that is capable of fitting multi-element data with sufficient accuracy and efficiency, without much human intervention. Second, even with the ML tools, a systematic and automatic procedure to generate uniformly accurate PES models, with a minimal set of training data, is still largely missing. The most straightforward approach is to perform extensive AIMD simulations at different temperatures and use them as training data for the energies and forces along the AIMD trajectories. However, this procedure is computationally demanding, and the generated snapshots are highly correlated, reducing the quality of the training data. For these reasons, a great amount of trial-and-error process is still involved in most of the ML-based PES models, and consequently, the reliability of these models is very much in doubt. In particular, even though there have been some efforts to build ML potential generation schemes for different materials,^{33–39} there lacks a well-benchmarked, automatic, and efficient potential generation scheme for superionic conductor materials.

In this study, we implement a concurrent learning scheme to generate uniformly accurate PES models for LiGePS-type superionic conductors. With the generated ML potentials, we establish a robust MD protocol to accurately estimate diffusion coefficients at room temperature. To represent the multi-element PES, we employ a smooth version of the Deep Potential (DP) model,²⁶ which is end-to-end, i.e. capable of fitting many-component data of SSE materials with little human intervention. Using the Deep Potential Generator (DP-GEN) scheme,^{40,41} a minimal set of training data is generated from an efficient and sufficient sampling of the relevant configuration space, thereby guaranteeing a reliable PES model produced by training.

We notice that a very recent work by Marcolongo et al³⁵ has used the DP model to study

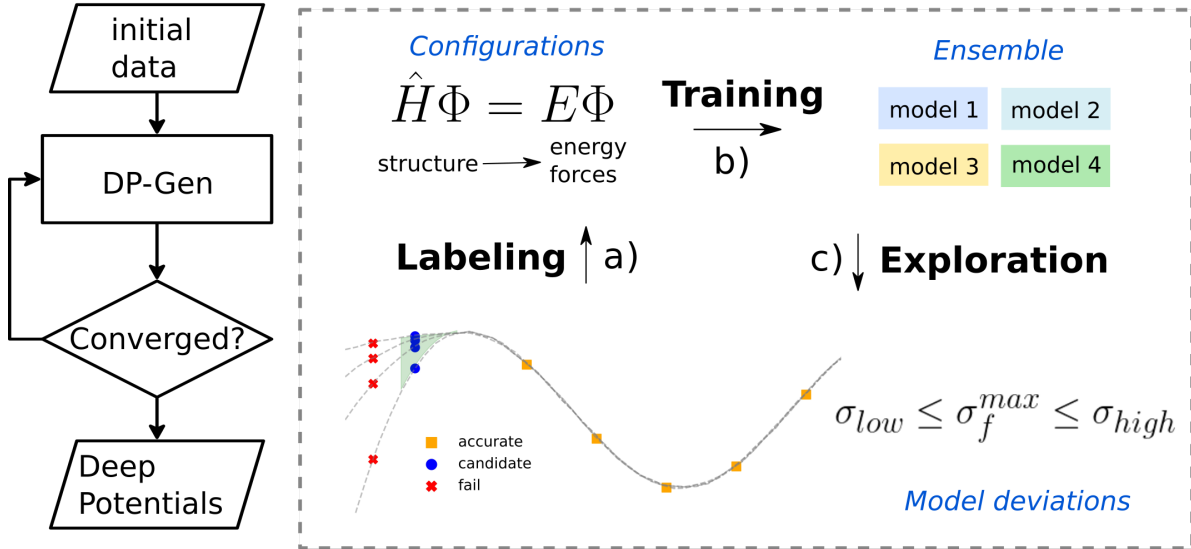


Figure 2: Flowchart of DP-GEN. To start DP-GEN, a dataset with hundreds of initial configurations is required. The iteration process is considered converged after a predetermined number of loops or only a small number (e.g. 0.1%) of new configurations are found in the last exploration process.

diffusion properties of solidstate electrolytes and proved by numerical results the reliability of DP predictions compared with AIMD. Here we shall focus on the data generation scheme and a systematic benchmark of the resulting DP models.

A brief description of the DP-GEN scheme is illustrated in Fig. 2. The iteration includes 3 stages: **labeling**, **training**, and **exploration**. (a) First, the dataset is **labeled** by running high precision single-point calculations. (b) Then, an ensemble of DP models with the same architecture (i.e. number of neural network layers and nodes) but different random seeds are **trained** using the whole training set. (c) To **explore** the configuration space, a few molecular dynamics simulations at different thermodynamic conditions are driven the DP models from the previous stage. Model deviations are evaluated using all trained models and new configurations are picked according to the maximum deviation of forces (σ_f^{max}), defined as:

$$\sigma_f^{max} = \max_i \sqrt{\langle ||f_i - \langle f_i \rangle||^2 \rangle}, \quad (1)$$

where f_i is the force acting on atom i , and $\langle \dots \rangle$ denotes the average of the DP model ensemble.

ble. Configurations with small force deviations ($\sigma_f^{max} < \sigma_{low}$, yellow square in Fig. 2(c)) are effectively covered by the training dataset with high probability. On the contrary, excessive force deviation ($\sigma_f^{max} > \sigma_{high}$, red cross in Fig. 2(c)) implies that the configuration may diverge from the relevant physical trajectories. Therefore none of them are picked. Only configurations whose σ_f^{max} fall between a predetermined window are labeled as *candidates* (blue circles in Fig. 2(c)). According to Ref.,⁴¹ a practical rule of thumb is to set σ_{low} slightly larger than the training error achieved by the model, and set σ_{high} 0.1-0.3 eV/Å higher than σ_{low} . Therefore, for all the examples in this paper, σ_{low} and σ_{high} are set to 0.12 and 0.25 eV/Å, respectively. In practice, after running several MD trajectories, the selection criterion usually produces hundreds or thousands of candidates. A small fraction of them is typically representative enough to improve the model, and therefore a cutoff number (N_{label}^{max}) is set to restrict the number of candidates. These candidates are then labeled and added to the original dataset for the next training. The labeling and training stages are rather standard, while there is large flexibility for the sampling strategy on how to explore the relevant phase space in each iteration. For example, different simulation times, system sizes, thermodynamic conditions, and sampling techniques can be used in different iterations.

The structures of LiGePS-type superionic conductors can be grouped into two subsystems: MS_4 ($M = Ge, Si, Sn$, and P) backbone blocks and mobile Li^+ ions. The solid-like backbone forms a sublattice, in which the liquid-like Li -ion is free to flow. The dynamics are characterized by the vibration of the backbone blocks and the diffusion of Li^+ between vacancies. These events can be efficiently captured by running MD at different temperatures. In practice, we start the DP-GEN iteration from 590 structures randomly perturbed around a DFT-relaxed crystalline structure. The exploration strategy of DP-GEN is to run plenty of low-cost DP-based MD and select candidates from the sampled snapshots. All explorations are conducted with 10 initial structures and 5 pressures simultaneously. In the first 4 iterations, the exploration time is gradually lengthened from 300 fs to 10000 fs (10 ps). Afterward, we use $2 \times 2 \times 2$ supercells for another 4 iterations with the same MD parameters.

The Deep Potential Generator scheme in this work was realized by the DP-GEN package.⁴¹ All DFT calculations were performed using the projector augmented-wave (PAW)⁴² method applied in VASP 5.4.4.^{43,44} We use the PBE scheme⁴⁵ for the functional approximation, a practice widely adopted in the investigation of SSE materials,¹⁰ and serves as a good benchmark. LAMMPS⁴⁶ was employed to run all MD simulation and DeePMD-kit⁴⁷ was used for training the DP model. More details of DPT, MD, as well as the DP-GEN setups can be found in the Supplementary Information (SI).

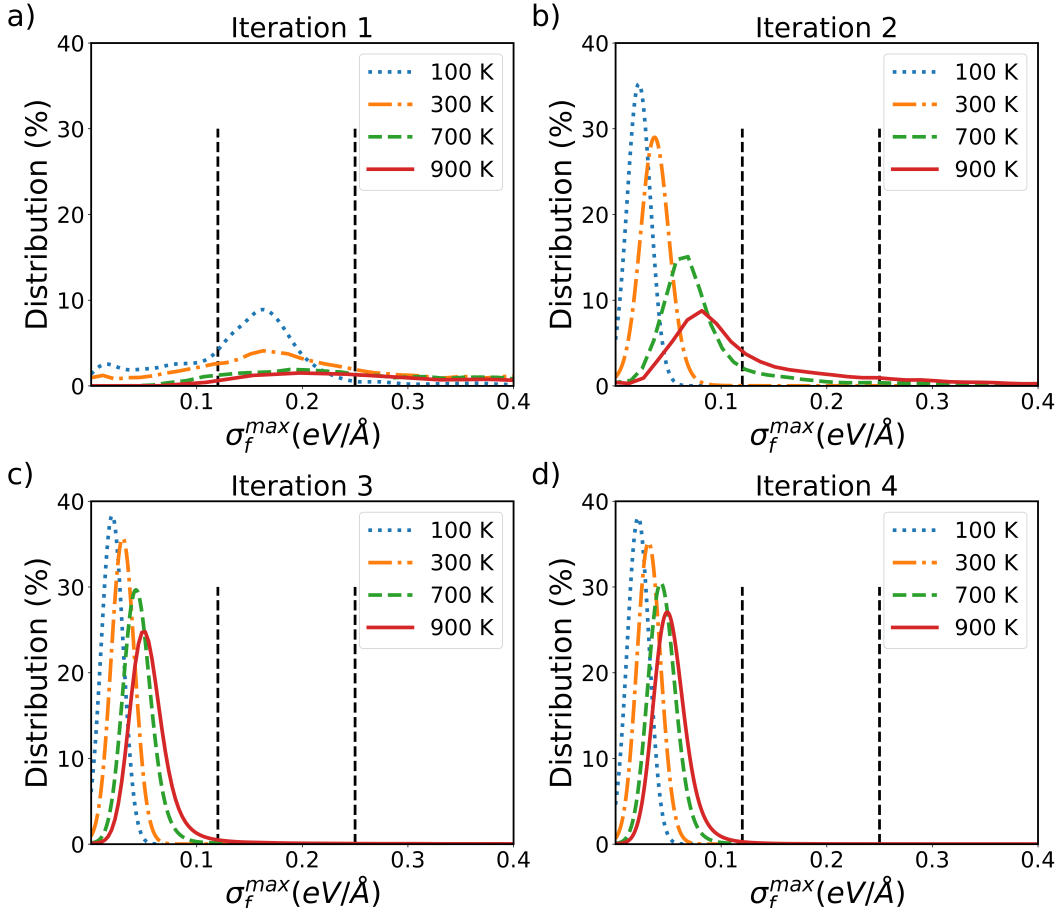


Figure 3: For $\text{Li}_{10}\text{GeP}_2\text{S}_{12}$, distribution of maximum deviation of force (σ_f^{max}) from iteration 1 to 4. Distribution of deviation values at 4 temperatures are plotted and the two vertical lines (dashed) correspond to the lower and upper bound of the selection criteria (0.12 and $0.25 \text{ eV}/\text{\AA}$).

To better illustrate the DP-GEN procedure, it is worth taking a thorough look at the exploration results from each iteration. As the first example, we study $\text{Li}_{10}\text{GeP}_2\text{S}_{12}$ in

depth due to its importance and extensive experimental reports. The same protocol is then extended to $\text{Li}_{10}\text{SiP}_2\text{S}_{12}$ and $\text{Li}_{10}\text{SnP}_2\text{S}_{12}$ to validate the efficiency of DP-GEN. Fig. 3 shows the distribution of σ_f^{max} at different temperatures in the first 4 iterations. During the 1st iteration, it is not surprising that the trajectories given by the preliminary models sample lots of unreasonable configurations and high-temperature simulations blow up very quickly. A large fraction of the snapshots sampled in this iteration have a σ_f^{max} larger than 0.4 eV/Å (Fig. 3 (a)). A large portion of the candidates selected for labelling are from low-temperature simulations. This situation is drastically improved after just adding 300 labeled configurations to the training dataset. In the 2nd iteration, most low-temperature snapshots are labeled as “accurate” and the majority of newly selected snapshots come from higher-temperature simulations. Going from the 2nd iteration to the 3rd and the 4th, although the time duration of the simulation is extended (i.e. 1000 fs, 5000 fs, and 10000 fs, respectively), most snapshots have their σ_f^{max} value at a satisfactory level, demonstrating a quick convergence of the DP-GEN process. After 4 iterations, the models have converged in the original cell (50 atoms), i.e. the percentage of candidates is $\sim 1\%$. (SI Table 2). The 5th to 8th iterations are performed with $2 \times 2 \times 2$ supercells (200 atoms) with the percentage of candidates gradually decreased to 0.6 %. In total, the DP-GEN scheme produced 2390 labeled configurations.

Table 1: Root-mean square error of the energies and forces of the DP models with training data generated from the DP-GEN procedure. The numbers in parentheses are the variance of the results, using different DP models, in the last digit.

System	$\text{Li}_{10}\text{GeP}_2\text{S}_{12}$	$\text{Li}_{10}\text{SiP}_2\text{S}_{12}$	$\text{Li}_{10}\text{SnP}_2\text{S}_{12}$
Energy (meV/atom)	1.65(4)	1.73(3)	1.44(1)
Force (meV/Å)	80.5(5)	79.0(6)	79.0(2)

After the DP-GEN procedure, we collect all the training data and use a “fine-training” to generate the production DP models (See SI for details). As shown in Table 1, the low deviation of the model ensemble suggests that the potentials have similar accuracy and the DP-GEN scheme gives consistent errors for 3 different systems. The root-mean-square errors

(RMSE) of energies and forces are around 2 meV/atom and 80 meV/Å, respectively. The volume of DP-relaxed $\text{Li}_{10}\text{GeP}_2\text{S}_{12}$ structure is 998.8 Å³, which agrees well with the DFT data (989.8 Å³). The resulting models are then used to study the simulation protocol for the diffusion properties. From now on, the discussion will be focused on the $\text{Li}_{10}\text{GeP}_2\text{S}_{12}$ system.

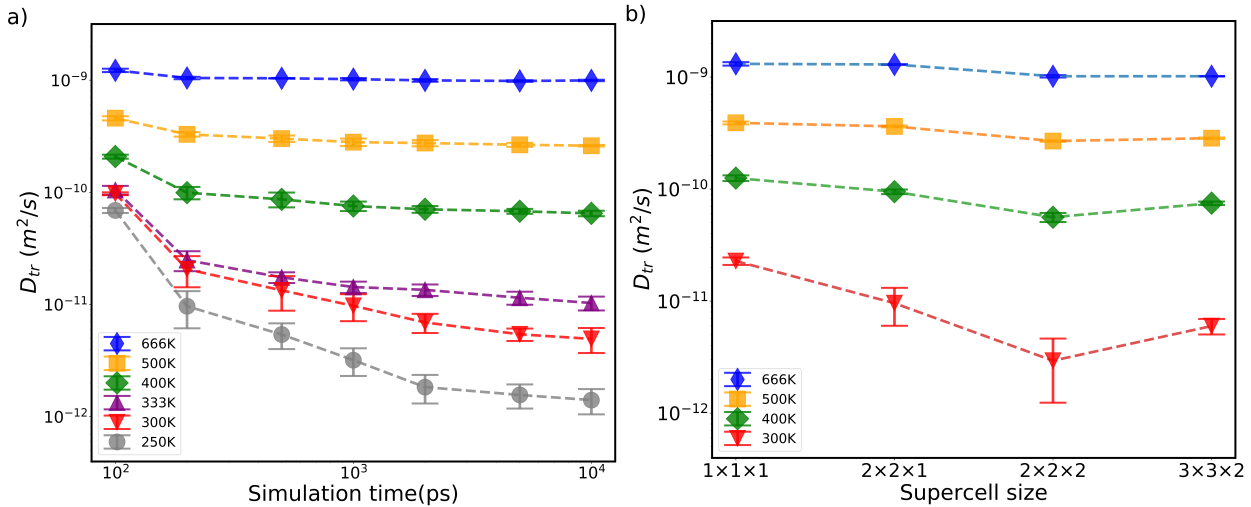


Figure 4: Diffusion coefficients of $\text{Li}_{10}\text{GeP}_2\text{S}_{12}$ calculated with different (a) simulation time length (100 ps, 200 ps, 500 ps, 1 ns, 2 ns, 5 ns and 10 ns) and (b) supercell size (50, 200, 400 and 900 atoms).

To investigate the statistical error of simulation time, we perform 10 ns simulations with $3 \times 3 \times 2$ supercell (900 atoms) at 6 temperatures (250 K, 300 K, 333 K, 400 K, 500 K, and 666 K). The tracer diffusion coefficient (D_{tr}) at each temperature is estimated by the time derivative of the mean-square displacement (MSD) of Li^+ . Previous studies¹⁶ based on AIMD have suggested that a 200 ps MD simulation would be sufficient to ensure the convergence of diffusivity at a high temperature ($>600\text{K}$). As shown in Fig. 4(a), we confirm that at 666K, the diffusivity data converge well within 200 ps, as expected. Diffusion coefficients above the level of $10^{-10}\text{m}^2/\text{s}$ (400 K, 500 K, and 666 K) reach very small variances and converge within 1 ns. However, since the diffusivity decreases exponentially with temperature, the statistics of diffusion processes at low temperatures requires much longer simulation time than that at high temperatures. At room temperature, extending the simulation time to

10 ns ensures convergence of all diffusivity data with the relative uncertainty of $10^{-12} \text{ m}^2/\text{s}$. Thus, we conclude that 10 ns is required for the simulation of room temperature diffusion processes.

Following the test for the simulation time, we also perform a similar analysis on the system size, using 10 ns trajectories. The system-size dependence of the diffusion coefficient and viscosity from MD simulations with periodic boundary conditions is a classic topic and has been extensively discussed by, e.g., Yeh et. al.⁴⁸ Here, as shown in Fig. 4(b), a $2 \times 2 \times 1$ supercell size, which was used in most previous AIMD simulations of SSE materials,^{12,15} gives decent result. To confirm this, we decide to run simulations with $3 \times 3 \times 2$ supercells for 10 ns to evaluate room temperature diffusivities. This was feasible since the DP model is several orders of magnitude faster than DFT. In fact, in contrast to the cubic scaling of DFT, the computational cost of DP scales linearly with the system size.

Another important factor, i.e. lattice parameter is known to significantly affect the diffusion process.^{49–51} In principle, one can simply equilibrate the simulation cell in an NpT ensemble and evaluate relevant quantities. However, considering the non-negligible difference between PBE-relaxed cell parameters and the experimental ones (see Table 4) we systematically evaluate the effect of lattice parameter upon diffusivity at low temperatures (below 700 K) by isotropically scaling the lattice volume from -5% to 5% and perform NVT MD simulations using DP. It is shown in Fig. 5 that such a tiny expansion or contraction is sufficient to lead to noticeable differences in the computed diffusion coefficients. This might be attributed to the geometrical change of the transport tunnel, which may further change the diffusion mechanism at some conditions. Volume expansion reduces the strong ionic bonds between lithium and sulfur, which benefits the hopping events. It may also weaken the repulsion between lithium ions, leading to the suppression of collective motion.

Since diffusivity is sensitive to lattice parameters, we also evaluate the temperature dependence of the lattice parameters in Figure 6 with 1-ns long NpT simulations. LiGePS-type materials belong to tetragonal crystal lattice, for which the lattice parameter a is equivalent

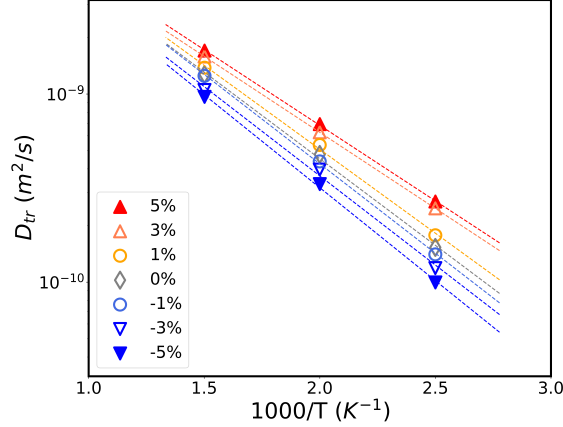


Figure 5: Diffusivity coefficients of $\text{Li}_{10}\text{GeP}_2\text{S}_{12}$ at 400K, 500K and 666K obtained with 1 ns NVT simulations. The lattice volumes are scaled to 95%, 97%, 99%, 100%, 101%, 103% and 105%, respectively.

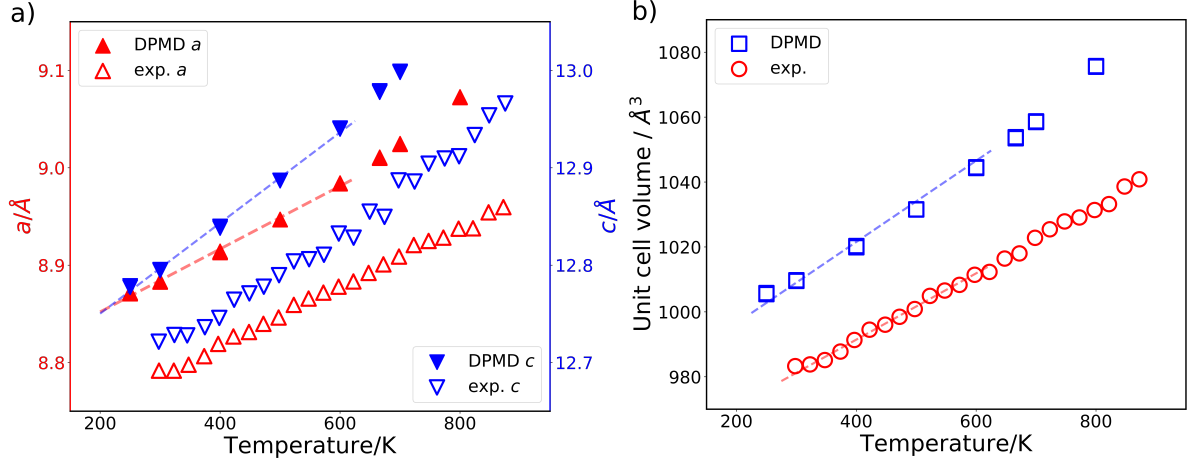


Figure 6: Thermal expansion of $\text{Li}_{10}\text{GeP}_2\text{S}_{12}$ at seven different temperatures (250 K, 300 K, 400 K, 500 K, 600 K, 666 K and 800K), (a) lattice parameters a and c ; (b) unit cell volumes. The dashed lines corresponding to the fitting range of thermal expansion coefficients. The experimental data is extracted from Weber et al.⁵²

to lattice parameter b , and thus the thermal expansion of lattice parameter a and c are presented. Weber et al⁵² found that lattice parameters a and c exhibit linear thermal expansion below 700 K and anisotropic expansion at higher temperature. Here we focus on the linear region that is of practical interest. The room temperature thermal expansion coefficient (α_{300K}^L) is $3.6 \times 10^{-5} \text{ K}^{-1}$, consistent with the value $3.5 \times 10^{-5} \text{ K}^{-1}$ from the literature.⁵²

Based on the investigation of the time and size convergence as well as the influence of the lattice parameters, in the current study for 3 different systems ($\text{Li}_{10}\text{GeP}_2\text{S}_{12}$, $\text{Li}_{10}\text{SiP}_2\text{S}_{12}$, and

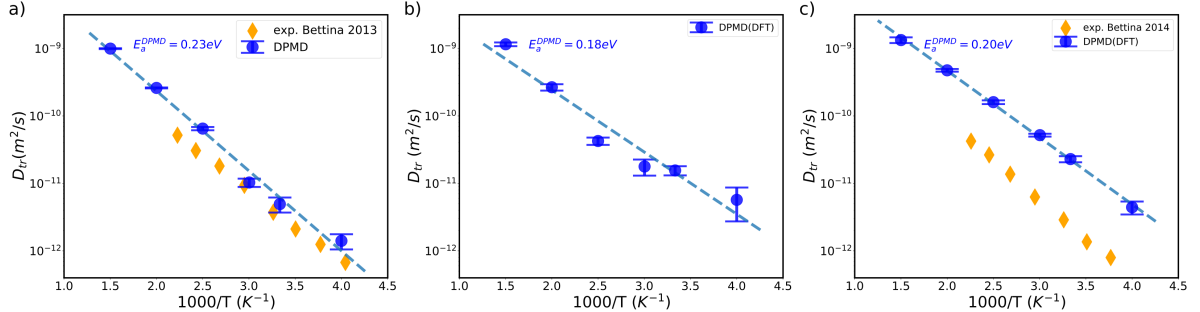


Figure 7: Temperature dependence of diffusion coefficients of (a) $\text{Li}_{10}\text{GeP}_2\text{S}_{12}$, (b) $\text{Li}_{10}\text{SiP}_2\text{S}_{12}$ and (c) $\text{Li}_{10}\text{SnP}_2\text{S}_{12}$, calculated by Deep Potential from 10 ns trajectories. Experimental results of $\text{Li}_{10}\text{GeP}_2\text{S}_{12}$ and $\text{Li}_{10}\text{SnP}_2\text{S}_{12}$ were extracted from NMR measurements.^{53,54}

$\text{Li}_{10}\text{SnP}_2\text{S}_{12}$), we run NVT simulation with DP models using experimental lattice parameters and with thermal expansion considered. The results are shown in Fig. 7. The activation energies of the three materials suggested by previous AIMD calculations are 0.21 ± 0.04 eV, 0.20 ± 0.03 eV and 0.24 ± 0.03 eV, respectively.⁴⁹ For $\text{Li}_{10}\text{GeP}_2\text{S}_{12}$, the room-temperature diffusion coefficient and activation energy calculated by Deep Potential are $D = 4.9 \times 10^{-12}$ m/s and $E_a = 0.23$ eV, in good agreement with the experimental data $D = 3.8 \times 10^{-12}$ m/s and $E_a = 0.22$ eV.⁵³ To the best of our knowledge, no relevant experimental data of the thermal expansion of $\text{Li}_{10}\text{SiP}_2\text{S}_{12}$ and $\text{Li}_{10}\text{SnP}_2\text{S}_{12}$ have been reported. Here we assume the two systems have similar thermal expansion coefficients as $\text{Li}_{10}\text{GeP}_2\text{S}_{12}$. The calculated activation energies (0.18 eV for $\text{Li}_{10}\text{SiP}_2\text{S}_{12}$ and 0.20 eV for $\text{Li}_{10}\text{SnP}_2\text{S}_{12}$) are slightly lower than the experimental value (0.20 eV for $\text{Li}_{10}\text{SiP}_2\text{S}_{12}$ and 0.27 eV for $\text{Li}_{10}\text{SnP}_2\text{S}_{12}$).^{55,56} While the agreement of diffusion coefficients of $\text{Li}_{10}\text{GeP}_2\text{S}_{12}$ between calculated and experimental results is very good, the same comparison on $\text{Li}_{10}\text{SnP}_2\text{S}_{12}$ shows a larger gap.

Several factors could contribute to the disagreement between the experimental and simulation results. First, the goal of involving machine-learning models is to extend the accessible simulation time and cell size without sacrificing accuracy. However, one needs to adopt a suitable functional approximation for DFT to provide training data that are accurate enough to describe relevant situations. Different functional approximations exhibit different descriptions of the bulk properties, the chemical bonding, etc.^{57,58} In Table 4 of SI we also calculated

the relaxed lattice parameters with different functional approximation schemes used in DFT (LDA,⁵⁹ PBEsol,⁶⁰ PBE with vdw correction⁶¹ and PBE0^{62,63}). These results suggest that PBEsol and PBE with vdw correction offer a better description of the lattice the volume. A more systematic investigation of the influence of the functional approximations is beyond the scope of this paper but would be facilitated by the accuracy and efficiency of DP and DP-GEN schemes. Secondly, the experimental tetragonal phase $\text{Li}_{10}\text{SiP}_2\text{S}_{12}$ is impure^{54,56} and the influence of the disorder seems to be more significant for $\text{Li}_{10}\text{SnP}_2\text{S}_{12}$,^{54,64} which might be the reason for the worse agreement between the simulation and experimental results for $\text{Li}_{10}\text{SnP}_2\text{S}_{12}$, compared with that for $\text{Li}_{10}\text{GeP}_2\text{S}_{12}$. We leave the investigation of these factors for future studies. Besides, the influence of defects and M-P site (M=Ge, Si, and Sn) disorder in LiGePS-type materials should be considered to further understand the diffusion processes.

In conclusion, we developed an efficient and automated workflow to generate ML potentials for $\text{Li}_{10}\text{GeP}_2\text{S}_{12}$ -type materials. Our focus in this paper is the validation of the simulation protocol. The effectiveness of the protocol is explained and analyzed in detail. We carefully studied the errors caused by limited simulation time and cell size. We also studied the lattice parameters and thermal expansion. We hope that this work represents a solid step forward towards the paradigm of generating a multi-component “universal potential” (i.e. Li-Ge-Si-Sn-P-S) to understand and design SSE with higher ionic conductivity.

Acknowledgement

J.-X. H. and J.C. are grateful for funding support from the National Natural Science Foundation of China (Grants No, 21861132015, 21991151, 91745103). J.-X. H. and J.-B. Z. are supported by the National Key Research and Development Program of China (Grant No. 2017YFB0102000). The work of L. Z. and W. E was supported in part by a gift from iFlytek to Princeton University, the ONR grant N00014-13-1-0338, and the Center Chemistry

in Solution and at Interfaces (CSI) funded by the DOE Award DE-SC0019394. The work of H. W. was supported by the National Science Foundation of China under Grant No. 11871110, the National Key Research and Development Program of China under Grants No. 2016YFB0201200 and No. 2016YFB0201203, and Beijing Academy of Artificial Intelligence (BAAI).

References

- (1) Goodenough, J. B.; Park, K.-S. The Li-ion rechargeable battery: a perspective. *Journal of the American Chemical Society* **2013**, *135*, 1167–1176.
- (2) Tarascon, J.-M.; Armand, M. *Materials for Sustainable Energy: A Collection of Peer-Reviewed Research and Review Articles from Nature Publishing Group*; World Scientific, 2011; pp 171–179.
- (3) Chu, S.; Majumdar, A. Opportunities and challenges for a sustainable energy future. *nature* **2012**, *488*, 294.
- (4) Hu, Y.-S. Batteries: getting solid. *Nature Energy* **2016**, *1*, 16042.
- (5) Zhang, Z.; Shao, Y.; Lotsch, B.; Hu, Y.-S.; Li, H.; Janek, J.; Nazar, L. F.; Nan, C.-W.; Maier, J.; Armand, M., et al. New horizons for inorganic solid state ion conductors. *Energy & Environmental Science* **2018**, *11*, 1945–1976.
- (6) Kamaya, N.; Homma, K.; Yamakawa, Y.; Hirayama, M.; Kanno, R.; Yonemura, M.; Kamiyama, T.; Kato, Y.; Hama, S.; Kawamoto, K., et al. A lithium superionic conductor. *Nature materials* **2011**, *10*, 682.
- (7) Murugan, R.; Thangadurai, V.; Weppner, W. Fast lithium ion conduction in garnet-type Li₇La₃Zr₂O₁₂. *Angewandte Chemie International Edition* **2007**, *46*, 7778–7781.

(8) Seino, Y.; Ota, T.; Takada, K.; Hayashi, A.; Tatsumisago, M. A sulphide lithium super ion conductor is superior to liquid ion conductors for use in rechargeable batteries. *Energy & Environmental Science* **2014**, *7*, 627–631.

(9) Car, R.; Parrinello, M. Unified approach for molecular dynamics and density-functional theory. *Physical Review Letters* **1985**, *55*, 2471.

(10) Ong, S. P.; Mo, Y.; Richards, W. D.; Miara, L.; Lee, H. S.; Ceder, G. Phase stability, electrochemical stability and ionic conductivity of the Li 10 ± 1 MP 2 X 12 (M= Ge, Si, Sn, Al or P, and X= O, S or Se) family of superionic conductors. *Energy & Environmental Science* **2013**, *6*, 148–156.

(11) Ceder, G.; Ong, S. P.; Wang, Y. Predictive modeling and design rules for solid electrolytes. *MRS Bulletin* **2018**, *43*, 746751.

(12) He, X.; Zhu, Y.; Mo, Y. Origin of fast ion diffusion in super-ionic conductors. *Nature communications* **2017**, *8*, 15893.

(13) Nolan, A. M.; Zhu, Y.; He, X.; Bai, Q.; Mo, Y. Computation-accelerated design of materials and interfaces for all-solid-state lithium-ion batteries. *Joule* **2018**,

(14) Van der Ven, A.; Ceder, G. Lithium diffusion in layered Li x CoO₂. *Electrochemical and Solid-State Letters* **2000**, *3*, 301–304.

(15) Mo, Y.; Ong, S. P.; Ceder, G. First Principles Study of the Li 10 GeP 2 S 12 Lithium Super Ionic Conductor Material. *Chemistry of Materials* **2012**, *24*, 15–17.

(16) He, X.; Zhu, Y.; Epstein, A.; Mo, Y. Statistical variances of diffusional properties from ab initio molecular dynamics simulations. *npj Computational Materials* **2018**, *4*, 18.

(17) Boyce, J. B.; Huberman, B. A. Superionic conductors: Transitions, structures, dynamics. *Physics Reports* **1979**, *51*, 189–265.

(18) Tachez, M.; Malugani, J.-P.; Mercier, R.; Robert, G. Ionic conductivity of and phase transition in lithium thiophosphate Li₃PS₄. *Solid State Ionics* **1984**, *14*, 181 – 185.

(19) Kwon, O.; Hirayama, M.; Suzuki, K.; Kato, Y.; Saito, T.; Yonemura, M.; Kamiyama, T.; Kanno, R. Synthesis, structure, and conduction mechanism of the lithium superionic conductor Li_{10+δ}Ge_{1+δ}P_{2-δ}S₁₂. *Journal of Materials Chemistry A* **2015**, *3*, 438–446.

(20) Kanno, R.; Murayama, M. Lithium Ionic Conductor Thio-LISICON: The Li 2S-GeS 2-P 2S 5 System. *Journal of the Electrochemical Society* **2001**, *148*, 742–746.

(21) Xiao, R.; Li, H.; Chen, L. Candidate structures for inorganic lithium solid-state electrolytes identified by high-throughput bond-valence calculations. *Journal of Materials* **2015**, *1*, 325–332.

(22) Kahle, L.; Marcolongo, A.; Marzari, N. Modeling lithium-ion solid-state electrolytes with a pinball model. *Physical Review Materials* **2018**, *2*, 065405.

(23) Behler, J.; Parrinello, M. Generalized neural-network representation of high-dimensional potential-energy surfaces. *Physical review letters* **2007**, *98*, 146401.

(24) Bartók, A. P.; Payne, M. C.; Kondor, R.; Csányi, G. Gaussian approximation potentials: The accuracy of quantum mechanics, without the electrons. *Physical review letters* **2010**, *104*, 136403.

(25) Artrith, N. The Atomic Energy Network (cnet)(release 2.0. 0). **2017**,

(26) Zhang, L.; Han, J.; Wang, H.; Saidi, W.; Car, R.; E, W. *Advances in Neural Information Processing Systems* **31**; Curran Associates, Inc., 2018; pp 4436–4446.

(27) Artrith, N.; Urban, A.; Ceder, G. Constructing first-principles phase diagrams of amorphous Li x Si using machine-learning-assisted sampling with an evolutionary algorithm. *The Journal of chemical physics* **2018**, *148*, 241711.

(28) Deringer, V. L.; Merlet, C.; Hu, Y.; Lee, T. H.; Kattirtzi, J. A.; Pecher, O.; Csányi, G.; Elliott, S. R.; Grey, C. P. Towards an atomistic understanding of disordered carbon electrode materials. *Chemical communications* **2018**, *54*, 5988–5991.

(29) Fujikake, S.; Deringer, V. L.; Lee, T. H.; Krynski, M.; Elliott, S. R.; Csányi, G. Gaussian approximation potential modeling of lithium intercalation in carbon nanostructures. *The Journal of chemical physics* **2018**, *148*, 241714.

(30) Lacivita, V.; Artrith, N.; Ceder, G. Structural and Compositional Factors That Control the Li-Ion Conductivity in LiPON Electrolytes. *Chemistry of Materials* **2018**, *30*, 7077–7090.

(31) Li, W.; Ando, Y.; Minamitani, E.; Watanabe, S. Study of Li atom diffusion in amorphous Li₃PO₄ with neural network potential. *The Journal of chemical physics* **2017**, *147*, 214106.

(32) Deng, Z.; Chen, C.; Li, X.-G.; Ong, S. P. An electrostatic spectral neighbor analysis potential for lithium nitride. *npj Computational Materials* **2019**, *5*, 75.

(33) Bernstein, N.; Csányi, G.; Deringer, V. L. De novo exploration and self-guided learning of potential-energy surfaces. *arXiv preprint arXiv:1905.10407* **2019**,

(34) Nyshadham, C.; Rupp, M.; Bekker, B.; Shapeev, A. V.; Mueller, T.; Rosenbrock, C. W.; Csányi, G.; Wingate, D. W.; Hart, G. L. Machine-learned multi-system surrogate models for materials prediction. *npj Computational Materials* **2019**, *5*, 1–6.

(35) Marcolongo, A.; Binninger, T.; Zipoli, F.; Laino, T. Simulating Diffusion Properties of Solid-State Electrolytes via a Neural Network Potential: Performance and Training Scheme. *ChemSystemsChem* *n/a*.

(36) Deringer, V. L.; Proserpio, D. M.; Csnyi, G.; Pickard, C. J. Data-driven learning and prediction of inorganic crystal structures. *Faraday Discuss.* **2018**, *211*, 45–59.

(37) Mortazavi, B.; Podryabinkin, E.; Novikov, I. S.; Roche, S.; Rabczuk, T.; Zhuang, X.; Shapeev, A. Efficient machine-learning based interatomic potentials for exploring thermal conductivity in two-dimensional materials. *Journal of Physics: Materials* **2020**,

(38) Podryabinkin, E. V.; Tikhonov, E. V.; Shapeev, A. V.; Oganov, A. R. Accelerating crystal structure prediction by machine-learning interatomic potentials with active learning. *Physical Review B* **2019**, *99*, 064114.

(39) Gubaev, K.; Podryabinkin, E. V.; Shapeev, A. V. Machine learning of molecular properties: Locality and active learning. *The Journal of Chemical Physics* **2018**, *148*, 241727.

(40) Zhang, L.; Lin, D.-Y.; Wang, H.; Car, R.; E, W. Active learning of uniformly accurate interatomic potentials for materials simulation. *Physical Review Materials* **2019**, *3*, 023804.

(41) Zhang, Y.; Wang, H.; Chen, W.; Zeng, J.; Zhang, L.; Wang, H.; E, W. DP-GEN: A concurrent learning platform for the generation of reliable deep learning based potential energy models. *Computer Physics Communications* **2020**, 107206.

(42) Blöchl, P. E. Projector augmented-wave method. *Physical review B* **1994**, *50*, 17953.

(43) Kresse, G.; Furthmüller, J. Efficient iterative schemes for ab initio total-energy calculations using a plane-wave basis set. *Physical review B* **1996**, *54*, 11169.

(44) Kresse, G.; Joubert, D. From ultrasoft pseudopotentials to the projector augmented-wave method. *Physical Review B* **1999**, *59*, 1758.

(45) Perdew, J. P.; Burke, K.; Ernzerhof, M. Generalized Gradient Approximation Made Simple. *Phys. Rev. Lett.* **1996**, *77*, 3865–3868.

(46) Plimpton, S. Fast parallel algorithms for short-range molecular dynamics. *Journal of computational physics* **1995**, *117*, 1–19.

(47) Wang, H.; Zhang, L.; Han, J.; E, W. DeePMD-kit: A deep learning package for many-body potential energy representation and molecular dynamics. *Computer Physics Communications* **2018**, *228*, 178–184.

(48) Yeh, I.-C.; Hummer, G. System-Size Dependence of Diffusion Coefficients and Viscosities from Molecular Dynamics Simulations with Periodic Boundary Conditions. *The Journal of Physical Chemistry B* **2004**, *108*, 15873–15879.

(49) Ong, S. P.; Mo, Y.; Richards, W. D.; Miara, L.; Lee, H. S.; Ceder, G. Phase stability, electrochemical stability and ionic conductivity of the Li₁₀+-1MP₂X₁₂ (M = Ge, Si, Sn, Al or P, and X = O, S or Se) family of superionic conductors. *Energy and Environmental Science* **2013**, *6*, 148–156.

(50) Bachman, J. C.; Muy, S.; Grimaud, A.; Chang, H.-H.; Pour, N.; Lux, S. F.; Paschos, O.; Maglia, F.; Lupart, S.; Lamp, P.; Giordano, L.; Shao-Horn, Y. Inorganic Solid-State Electrolytes for Lithium Batteries: Mechanisms and Properties Governing Ion Conduction. *Chemical Reviews* **2016**, *116*, 140–162, PMID: 26713396.

(51) Fitzhugh, W.; Ye, L.; Li, X. The effects of mechanical constriction on the operation of sulfide based solid-state batteries. *J. Mater. Chem. A* **2019**, *7*, 23604–23627.

(52) Weber, D. A.; Senyshyn, A.; Weldert, K. S.; Wenzel, S.; Zhang, W.; Kaiser, R.; Berendts, S.; Janek, J.; Zeier, W. G. Structural Insights and 3D Diffusion Pathways within the Lithium Superionic Conductor Li₁₀GeP₂S₁₂. *Chemistry of Materials* **2016**, *28*, 5905–5915.

(53) Kuhn, A.; Duppel, V.; Lotsch, B. V. Tetragonal Li₁₀GeP₂S₁₂ and Li₇GePS₈ exploring the Li ion dynamics in LGPS Li electrolytes. *Energy Environ. Sci.* **2013**, *6*, 3548–3552.

(54) Kuhn, A.; Gerbig, O.; Zhu, C.; Falkenberg, F.; Maier, J.; Lotsch, B. V. A new ultra-fast superionic Li-conductor: ion dynamics in Li₁₁Si₂PS₁₂ and comparison with other tetragonal LGPS-type electrolytes. *Phys. Chem. Chem. Phys.* **2014**, *16*, 14669–14674.

(55) Bron, P.; Johansson, S.; Zick, K.; Schmedt auf der Gnne, J.; Dehnen, S.; Roling, B. Li₁₀SnP₂S₁₂: an affordable lithium superionic conductor. *Journal of the American Chemical Society* **2013**, *135*, 15694–15697.

(56) Whiteley, J. M.; Woo, J. H.; Hu, E.; Nam, K.-W.; Lee, S.-H. Empowering the lithium metal battery through a silicon-based superionic conductor. *Journal of the Electrochemical Society* **2014**, *161*, A1812–A1817.

(57) Wang, Z. Q.; Wu, M. S.; Liu, G.; Lei, X. L.; Xu, B.; Ouyang, C. Y. Elastic properties of new solid state electrolyte material Li₁₀GeP₂S₁₂: A study from first-principles calculations. *International Journal of Electrochemical Science* **2014**, *9*, 562–568.

(58) Hu, C. H.; Wang, Z. Q.; Sun, Z. Y.; Ouyang, C. Y. Insights into structural stability and Li superionic conductivity of Li₁₀GeP₂S₁₂ from first-principles calculations. *Chemical Physics Letters* **2014**, *591*, 16–20.

(59) Kohn, W.; Sham, L. J. Self-Consistent Equations Including Exchange and Correlation Effects. *Phys. Rev.* **1965**, *140*, A1133–A1138.

(60) Perdew, J. P.; Ruzsinszky, A.; Csonka, G. I.; Vydrov, O. A.; Scuseria, G. E.; Constantin, L. A.; Zhou, X.; Burke, K. Restoring the Density-Gradient Expansion for Exchange in Solids and Surfaces. *Phys. Rev. Lett.* **2008**, *100*, 136406.

(61) Klimeš, J.; Bowler, D. R.; Michaelides, A. Chemical accuracy for the van der Waals density functional. *Journal of Physics: Condensed Matter* **2009**, *22*, 022201.

(62) Perdew, J. P.; Ernzerhof, M.; Burke, K. Rationale for mixing exact exchange with density functional approximations. *The Journal of Chemical Physics* **1996**, *105*, 9982–9985.

(63) Adamo, C.; Barone, V. Toward reliable density functional methods without adjustable parameters: The PBE0 model. *The Journal of Chemical Physics* **1999**, *110*, 6158–6170.

(64) Kuhn, A.; Köhler, J.; Lotsch, B. V. Single-crystal X-ray structure analysis of the superionic conductor Li₁₀GeP₂S₁₂. *Physical Chemistry Chemical Physics* **2013**, *15*, 11620.